



Asymmetric scattering effect of solitary wave in a two-section composite granular chain

Xingyi Liu · Tengfei Jiao · Shutian Zhang ·
Min Sun · Decai Huang 

Received: 12 December 2023 / Accepted: 29 January 2024 / Published online: 1 March 2024
© The Author(s), under exclusive licence to Springer Nature B.V. 2024

Abstract Granular chain serves as a fundamental component for controlling the nonlinear solitary wave propagation in acoustic metamaterials. The understanding of the nonlinear scattering at the mismatched interface plays a crucial role in designing novel acoustic devices. In this study, numerical simulations are conducted to investigate the asymmetric scattering effect of solitary waves in a two-section composite granular chain. Building upon Nesterenko's work on solitary waves in monodisperse granular chains and using continuous acoustic wave theory in linear medium, we argue that the mismatches of acoustic velocity and acoustic impedance, because of the differences of mass density and elastic coefficient, dominate the asymmetric scattering effect at the mismatched interface. The simulation results confirm the occurrence of a multipulse structure for the transmitted solitary waves when the solitary wave passes through the mismatched interface with a small–large wave velocity. The overshooting effect occurs for the reflected solitary waves because of the mismatched interface with high–low acoustic impedance. The phase diagram in the space of the mass density and the elastic coefficient ratio of the right-section granular chain to the left-section granular chain further validates the predictions.

Keywords Granular Materials · Mechanics of discrete system · Asymmetric scattering · Discrete element method

1 Introduction

Granular materials, consisting of discrete grains, are commonly encountered in agricultural and industrial activities. These materials exhibit various unique phenomena such as dilute-dense granular flow and segregation of binary mixtures. [1–6] These phenomena have been extensively observed in grain storage, pharmaceutical mixing, mineral exploitation, and mechanical processing. The ordered granular chain (GC) is a fundamental component used to control and manipulate the propagation of mechanical waves in numerous applications. [7–16] This includes energy management, signal processing, shock mitigation, and even the design of mechanical logic elements. Understanding the dynamics of nonlinear wave propagation, especially nonlinear scattering at mismatched interfaces, within an ordered granular chain is crucial for theoretical investigations and engineering applications in the field of acoustic metamaterials.

One-dimensional GC with monodisperse elastic spheres is a good candidate for investigating wave propagation dynamics. Hertz model without energy dissipation is a classical model describing the nonlinear interaction force between the touching spherical grains, i.e., $F = k_n \delta^{3/2}$, where k_n is the elastic coefficient and δ is

X. Liu · T. Jiao · S. Zhang · M. Sun · D. Huang (✉)
Department of Applied Physics, Nanjing University of Science and Technology, Nanjing 210094, China
e-mail: hdc@njjust.edu.cn

the overlap of contact. Nesterenko conducted a pioneering work on the propagation of an instantaneous pulse in an ideal homogeneous GC. [17–19] In an extreme case, the GC is strongly precompressed, and in the other one, precompression is absent. For the former, a KdV equation is derived. Thus, a solitary wave (SW) solution is obtained for the first time. For the latter, the numerical simulation result proves the existence of SW even though the equation cannot be analytically solved. Thus, much work was performed on the propagation dynamics of SW in GC. [20–24] The validated propagation characteristics of SW in GC are the same as those in continuous fluid. [25–27] For example, the incident impulse is finally transformed into a stable SW, which means that the SW can propagate without any scattering in both unprecompressed and strongly precompressed granular chains (GCs). The larger amplitude of SW has a higher wave velocity. Moreover, many of the atypical characteristics of SW in GC are sequentially discovered. The unprecompressed GC cannot support the acoustic wave, which is commonly called as the sonic-vacuum one. When an external precompression is loaded, the amplitude of SW can be tuned because of the introduction of a nonlinear scattering effect. [28–31] Hence, how the nonlinear scattering effect affects the SW propagation characteristic has become a hot topic in the past decades.

SW is a highly localized wave that leads to a unique nonlinear scattering effect in continuous liquid, [32] optical system, [33], Toda lattice [34], etc. Given the intrinsic characteristic of Hertz interaction law between the touching spherical grains in GC, two kinds of nonlinear scattering effects attracted much concern in numerical simulations and experimental explorations. The first kind of effects is focused on the influence of the collision of two identical solitary waves (SWs) on the nonlinear scattering effect. For two head-on collision SWs, a train of secondary solitary waves arise because of the nonlinear scattering when the precompression is absent. [35–39] Compared with the effect of freely propagating SW, the nonlinear scattering effect can lead to an occurrence of leading phase shift for two head-collision ideal SWs. [40–44] When the amplitudes of two SWs are unequal, the low-energy SW gains a part of the energy from the high-energy one for the two head-on collision SWs; however, the scattering results are completely reversed for the overtaking case. [45,46]

The other concern on the nonlinear scattering effect is concentrated on intrinsic material properties, i.e.,

mass density and elastic coefficient. [47–54] Vergara numerically studied two sonic-vacuum composite GCs with different masses. [47] The mass-mismatch interface leads to the breakdown of the incident SW (ISW). The transmitted SWs (TSWs) and the reflected SWs (RSWs) are generated for the light-heavy chain. However, only the TSWs are observed for the heavy-light chain, in which the fracture of the ISW occurs and a multipulse-structure TSW arises. Similarly, the mismatch of the elastic coefficient is also used to tune this nonlinear asymmetric scattering effect. Nesterenko et al. established an experiment setup and corresponding simulation system, which is a vertical two-section composite GC comprising of a column of stainless steel spheres at the top section and a column of PTFE spheres at the bottom section. [48] The mismatched interface of acoustic impedance results in the formation of an acoustic diode effect. No reflected wave is detected when the stainless steel spheres are not magnetized. However, when the external magnetic field is applied, the compressive RSWs have a leading SW and a train of tailed oscillatory waves. According to continuous acoustic wave theory in a linear medium, it has been well known that the scattering results are determined by two critical acoustic quantities, i.e., acoustic velocity and acoustic impedance. The former leads to the expansion or squeezing of ISW at the mismatched interface, and the reflected energy coefficient can be analytically derived from the latter [55,56]. As far as we know, no systematic studies have been conducted to validate linear medium theory on the nonlinear asymmetric scattering effect of SW in a two-section composite GC. Further study on the nonlinear scattering effect of SW due to the mismatched interface is crucial to the improved understanding of SW scattering properties.

The current study provides simulations on a two-section composite GC with mismatched mass density and elastic coefficient. A single SW occurs from the left section of GC. Section 2 describes the simulation model and used parameters. Section 3 briefly revisits the Nesterenko work of monodisperse GC at the unprecompressed and precompressed conditions. Then, an argument is proposed using linear medium theory. Section 4 shows the detailed nonlinear asymmetric scattering effect in unprecompressed and precompressed composite GCs. The phase diagram in the mass density and elastic coefficient is then plotted. Then, the corresponding energy scattering is discussed for four typical cases. Section 5 summarizes the conclusions.

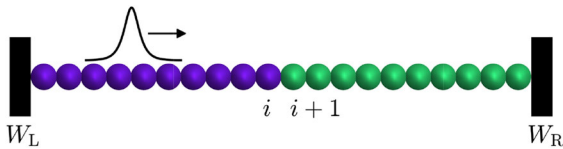


Fig. 1 Sketch of a two-section composite granular chain

2 Simulation model

Figure 1 shows the sketch of a one-dimensional composite GC with two sections. A line of spherical grains $N = N_L + N_R$ with identical diameter $d = 5$ mm is arranged between two fixed walls, i.e., W_L and W_R . N_L and N_R denote the grain numbers of the left and the right sections, respectively. In the simulation, the precompression is achieved by adjusting the distance between the left and the right walls. The interaction force without dissipation between two adjacent grains is only considered in the normal direction. Hertz model is used to describe the nonlinear interaction [57–59],

$$F_i^H = k_n[\delta_0 + (u_{i-1} - u_i)]_+^{3/2}, \tag{1}$$

where $[\cdot]_+ = \max[0, \delta_0 + (u_{i-1} - u_i)]$. i is the index of the grain. δ_0 is the precompression between the adjacent grains. u_i denotes the displacement of i th grain from equilibrium position. k_n is the elastic coefficient $k_n = \frac{2E}{3(1-\nu^2)}d^{1/2}$. E is the Young’s modulus and ν is the Poisson ratio. The interaction force between the grain and the wall is treated as the grain–grain interaction except that the wall has an infinite mass. $m = \frac{4}{3}\pi(d/2)^3\rho$ is grain mass, and ρ is mass density. The parameters of granular materials in the left-section GC used in the simulations are listed in Table 1. Here, $\alpha_\rho = \rho^R/\rho^L$ and $\alpha_{k_n} = k_n^R/k_n^L$ are defined as the ratios of mass density and elastic coefficient in the right and the left sections of GC. The composite GC is named as the heavy–light GC for $\alpha_\rho < 1$ and the light–heavy GC for $\alpha_\rho > 1$, respectively. Similarly, hard–soft GC and soft–hard GC are defined for $\alpha_{k_n} < 1$ and $\alpha_{k_n} > 1$, respectively. Obviously, GC is a monodisperse one for $\alpha_\rho = 1$ and $\alpha_{k_n} = 1$.

In the simulation, the discrete element method is adopted to describe the motion of each grain. The position and velocity of each grain are updated by integrating Newton’s second law of motion. The Verlet-velocity algorithm is used in each time step. [3,6,9,64]

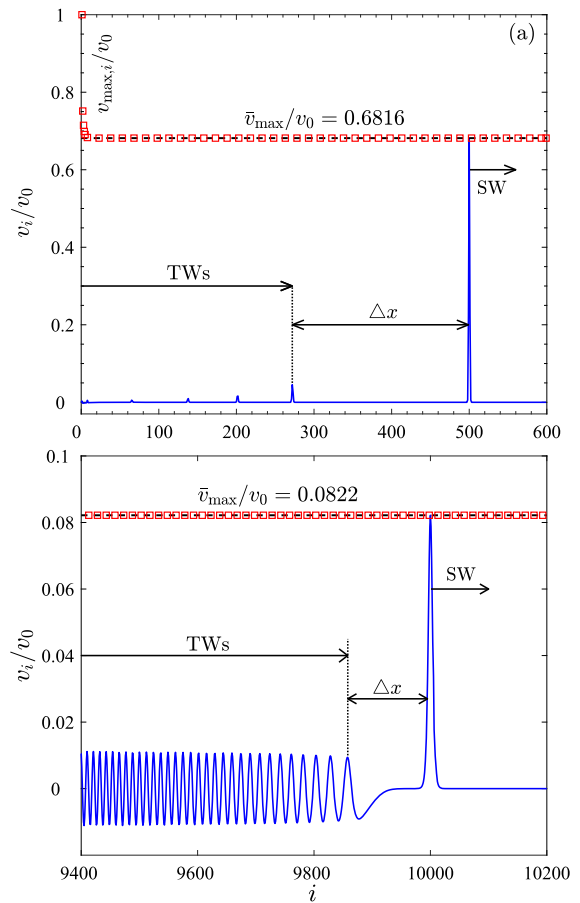


Fig. 2 Solitary wave and tailed waves in a monodisperse GC with precompression of **a** $\delta_0/d = 0$ and **b** $\delta_0/d = 10^{-3}$. Squares are the maximum grain velocity when solitary wave passes by and the dashed line is its average

According to Eq.(1), grain i moves under the following equation,

$$m \frac{d^2 u_i(t)}{dt^2} = k_n[\delta_0 + (u_{i-1} - u_i)]_+^{3/2} - k_n[\delta_0 + (u_i - u_{i+1})]_+^{3/2}. \tag{2}$$

An instantaneous pulse is introduced by giving a velocity of left-most grain ($v_0 = 1$ m/s) to produce an SW in monodisperse GC. Moreover, the others are static. As shown in Fig. 2, the instantaneous pulse is extended after a traveling distance and a leading front SW is clearly observed followed by a series of tailed waves (TWs). For $\delta_0 = 0$, the TWs are composed of many discrete SWs, and they are a train of oscillatory waves being diminishing for $\delta_0/d = 10^{-3}$. The trav-

Table 1 The parameters of the granular materials

Quantity	Symbol	Value
Diameter (mm)	d	5
Density for grain (g/cm ³)	ρ	7.9
Young's modulus (GPa)	E	193
Poisson's ratio	ν	0.25
Simulation time-step (s)	dt	10^{-9}

eling distance necessary to form a leading front SW in the latter is larger than that in the former. Furthermore, the farther the SW travels, the wider the distance (Δx) is between the SW and the first peak of TWs. In Fig. 2, the amplitude of grain velocity is plotted as a function of grain number and it becomes a constant value as the propagation progresses. v_{\max} is the maximum grain velocity of the SW and \bar{v}_{\max} denotes its average. \bar{v}_{\max}/v_0 is 0.6816 and 0.0822 for $\delta_0/d = 0$ and 10^{-3} , respectively. After the SW has passed through, the grain reaches its maximum displacement. The average is recorded as \bar{u}_{\max} . In the following simulations, only the SW is translated to the left section of the composite GC and the velocities of other grains are set to zero at the beginning.

3 Theoretical arguments

3.1 Nesterenko's theory of the solitary wave

In the study of GC, both mass density and elastic coefficient have been found to play critical roles in the propagation dynamics of the SW [17–19, 28, 47, 53]. Here we briefly highlight Nesterenko's pioneered explorations on the unique characteristic of SW in GC [17–19]. A strongly precompressed GC is first considered, $|u_i - u_{i+1}|/\delta_0 \ll 1$. Taylor expansion is used and Eq. (2) can be rewritten as:

$$\frac{d^2 u_i(t)}{dt^2} = \alpha(u_{i-1} - 2u_i + u_{i+1}) + \beta(u_{i-1} - 2u_i + u_{i+1})(u_{i-1} - u_{i+1}),$$

$$N - 1 > i \geq 2, \quad \alpha = \frac{3k_n}{2m} \delta_0^{1/2}, \quad \beta = \frac{3k_n}{8m} \delta_0^{-1/2}. \quad (3)$$

Nesterenko employs a continuum approximation with $L > d$, where L is the characteristic spatial size

of the perturbation to make Eq. (3) into a classical KdV equation,

$$u_{tt} = c_0^2(u_{xx} + au_{xxx} - bu_x u_{xx}),$$

$$c_0^2 = \frac{3k_n}{2m} d^2 \delta_0^{1/2}, \quad a = \frac{d^2}{12}, \quad b = \frac{d}{\delta_0}, \quad (4)$$

where the terms of $O((\frac{d}{L})^4)$ and high-order terms are ignored. Equation 4. c_0 is considered the characteristic acoustic velocity for precompressed GC. The corresponding SW velocity is analytically derived:

$$V_S = c_0 \left(1 + \frac{d\xi_{\max}}{12\delta_0} \right), \quad (5)$$

where ξ_{\max} is the maximum strain of moving grains in SW.

The other analysis is conducted for the weakly precompressed GC with $|u_i - u_{i+1}|/\delta_0 \gg 1$. It begins at $\delta_0 \sim u_i - u_{i+1}$ as an initial condition. Thus, the equation of motion for grain i is:

$$m \frac{d^2 u_i(t)}{dt^2} = k_n \left[(u_{i-1} - u_i)^{3/2} - (u_i - u_{i+1})^{3/2} \right], \quad (6)$$

Hence, it is ready for a long wavelength approximation where u_{i-1} and u_{i+1} in Eq. (6) can be expanded in a power series using a small parameter $\epsilon = d/L$. Nesterenko conducted a fourth-order expansion to eventually obtain the formidable nonlinear equation

$$u_{tt} = c^2 \left[\frac{3}{2} (-u_x)^{1/2} u_{xx} + \frac{d^2}{8} (-u_x)^{1/2} u_{xxx} - \frac{d^2}{8} \frac{u_x u_{xxx}}{(-u_x)^{1/2}} - \frac{d^2}{64} \frac{(u_{xx})^3}{(-u_x)^{3/2}} \right],$$

$$-u_x > 0, \quad c_{\text{mat}}^2 = \frac{k_n}{m} d^{5/2}. \quad (7)$$

where c_{mat} is the acoustic wave velocity of bulk materials. Nesterenko simplified Eq. (7) and proposed an SW solution, which appears to be consistent with the experiments at an unprecompressed condition, $\delta_0 = 0$. The width of SW was found to be about $10R$, which compares well with experiments. The SW velocity is written as,

$$V_{S0} = \frac{2}{\sqrt{5}} c_{\text{mat}} \xi_{\text{max}}^{1/4}, \tag{8}$$

The validity of Eqs.(5)(8) has been confirmed in several studies [22,28,40,49]. The characteristic wave velocities, c_0 and c_{mat} , and the maximum strain, ξ_{max} , are crucial factors for determining the SW dynamics in the GC. Our previous studies showed that the former is highly correlated with the intrinsic dynamics of SW, whereas the latter controls the velocity magnitude of SW [31,42]. Therefore, exploring the influence of the characteristic wave velocities on the scattering effect at the mismatched interface is noteworthy.

3.2 Acoustic wave theory in linear medium

When the ISW passes through a mismatched interface, $x = 0$, the grains around the interface must be involved simultaneously because the SW has a certain width. In our simulation, the deformation induced by ISW is rather smaller contrasted with the initial pre-compression, δ_0 for a small amplitude of ISW. Thus, the ISW can be considered traveling across a pre-compressed two-section composite GC with different material parameters. Mass density and elastic coefficient are regarded to remain constant. In particular, Eqs.(5)(8) indicate that mass density and elastic coefficient have the same effects on the characteristic wave velocities c_0 and c_{mat} . Thus, we can make the following arguments on the asymmetric scattering effect taken from the mismatched mass density and elastic coefficient by using classical acoustic theory in a linear medium.

First, the characteristic wave velocity ratio of the c_0^R of the right section to c_0^L of the left section is introduced,

$$\gamma_{c_0} = c_0^R / c_0^L = \alpha_\rho^{-1/2} \alpha_{k_n}^{1/3}, \tag{9}$$

in which the initial force equilibrium condition is used, $k_n^L (\delta_0^L)^{3/2} = k_n^R (\delta_0^R)^{3/2}$.

Second, the continuity boundary condition validates for the pressure and grain velocity at the mismatched interface of two-section composite GC.

$$(P_{\text{In}})_{x=0} + (P_{\text{Re}})_{x=0} = (P_{\text{Tr}})_{x=0}, \tag{10a}$$

$$(v_{\text{In}})_{x=0} + (v_{\text{Re}})_{x=0} = (v_{\text{Tr}})_{x=0}. \tag{10b}$$

According to the relation between the acoustic pressure and grain velocity, i.e., $v = -\frac{1}{\rho_0} \int \frac{\partial P}{\partial x} dt$, Eq. (10) can be rewritten for the case of two-section composite GC:

$$P_{\text{In}}^L + P_{\text{Re}}^L = P_{\text{Tr}}^R, \tag{11a}$$

$$\frac{P_{\text{In}}^L}{R_G^L} - \frac{P_{\text{Re}}^L}{R_G^L} = \frac{P_{\text{Tr}}^R}{R_G^R}. \tag{11b}$$

where $R_G = \rho_0 c_0$ is another key physical quantity, the acoustic impedance, on the scattering effect.

Thus, the acoustic pressure ratios of the transmitted and the incident waves can be defined as:

$$\frac{P_{\text{Tr}}^R}{P_{\text{In}}^L} = \frac{2}{1 + \gamma_{R_G}^{-1}}. \tag{12}$$

in which the ratio of acoustic impedance of right section to that of left can be obtained using Eq. (9),

$$\gamma_{R_G} = R_G^R / R_G^L = \alpha_\rho^{1/2} \alpha_{k_n}^{1/3}. \tag{13}$$

Introducing of the characteristic wave velocity ratio and the acoustic impedance ratio is useful for discussing the asymmetric scattering effect in the two-section composite GC with a mismatched interface. First, the mismatch of wave velocity can lead to the “fracture” and “squeeze” effects of the ISW at the interface for $\gamma_{c_0} > 1$ and $\gamma_{c_0} < 1$, respectively. At the former condition, the single-peak ISW decomposes into at least two parts because the leading front ISW first passing across the interface has a larger propagation velocity in the right-section GC than that the following part lagging in the left-section GC. Under the latter condition, the propagation velocity of the leading front ISW in the right-section GC is smaller than that of the following part in the left-section GC. The two parts would be squeezed, and thus, compressive TSWs and RSWs are generated on both sides of the interface of the two-section GC. Second, the mismatch of the acoustic

impedance can also result in ISW breakdown. Compared with the “soft” right-section GC, the left-section GC can be considered as a “hard” one when $\gamma_{RG} < 1$. In this case, the acoustic pressure of the transmitted wave P_{Tr}^R is lower than the incident wave P_{In}^L . This indicates the occurrence of the overshooting phenomenon when the grains in the RSWs keep the same phase as that in the ISW. The RSWs should be an expansive wave. Under the condition of $\gamma_{RG} > 1$, $P_{Tr}^R/P_{In}^L > 1$, P_{Re}^L is higher than zero. The left-section GC is “soft”, making the RSWs and the TSWs being compressive [55, 56, 60, 61]. When $\gamma_{RG} = 1$, the reflection is completely suppressed and total transmission occurs.

4 Simulation results

First, the simulations were conducted to explore the asymmetric scattering effect in a two-section composite GC with different mass densities. The precompression is set to $\delta_0 = 0$. In Fig. 3a, a heavy–light GC is used. The ratio of mass density is $\alpha_\rho = \rho^R/\rho^L = 0.2$, i.e., $\gamma_{c0} > 1$ and $\gamma_{RG} < 1$. The mismatched interface is placed between grains 400 and 401. Grain velocity is plotted as a function of grain number when the center of the front wave of TSWs(FTSW) arrives at grain 550. The mass–mismatch interface leads to occurrence of a wave fracture in the right-section GC [47], in which a series of multipulse-structure TSWs arises. These separated TSWs obviously have two distinct parts, 1st and 2nd, and they have a leading front wave with large amplitude and a train of isolated TWs with gradually decreasing amplitude, respectively. The definitions of 1st and 2nd are explained in the following. The other notable result is that the nonlinear scattering effect only occurs in the right-section GC. All grains in the left-section GC remain static. However, those around the interface have a very tiny forward motion, indicating that no reflection appears.

The same simulations were performed on a light–heavy GC with $\alpha_\rho = 5$, i.e., $\gamma_{c0} < 1$ and $\gamma_{RG} > 1$. The results are plotted in Fig. 3b. Compared with the heavy–light interface, the light–heavy one extends the nonlinear scattering effect to both sides of the interface. In the right–section GC, the TSWs still have two parts, 1st and 2nd. The former is composed of a single FTSW, which occupies most of the energy of TSWs. The latter is too weak to be visible. A train of RSWs are observed in the left-section GC. It also has two parts,

1st and 2nd. The former has only one single front wave of RSWs(FRSW) and the later is an SW train. In addition, the amplitude of the FRSW is much larger than that following the waves of the 2nd. Here, the grains in the RSWs have negative velocities, indicating that the RSWs are compressive waves.

Figure 3c, d plots the temporal evolution of the grain displacement around the interface at the same simulations in Fig. 3a, b to understand the origin of mass-mismatch-induced nonlinear asymmetric scattering phenomena, respectively. The slope of the displacement–time curve corresponds to grain velocity. The velocity is zero when the displacement–time curve is a horizontal straight line. This scenario means that the grain is static. When the displacement–time curve is an inclined straight line, the grain moves freely at a constant velocity and loses contact with its adjacent neighbors. A positive slope indicates that the grain keeps moving forward, whereas a negative slope denotes that the grain is reflected back.

In Fig. 3c, no scattering effect occurs when the grain is far from the mass–mismatch interface, such as grain 395. Moreover, the ISW passes across the interface freely in the initial form. Two moving modes appear in turn. The contact-move mode first occurs, in which grain 395 keeps contact with its adjacent grains, i.e., grain 394 and 396, and it moves forward in the propagation direction of the ISW. After the passage of the ISW, grain 395 reaches its maximum displacement and remains at static, namely as static mode [62]. When the ISW arrives at the heavy–light interface, the collision between grain 400 and grain 401 occurs for the first time. Initially, the grains around the interface, i.e., heavy grains 399 and 400 in the left section and light grains 401 and 402 in the right section, move forward together in the contact-move mode. Owing to mass mismatch, grain 399 first reaches its larger displacement and enters into the forward free-flight move mode for the first time, marked as 1st free flight. However, the overshooting effect occurs for grain 400 because of its heavy mass, and it continues to move forward together with light grains 401 and 402. This phenomenon increases the amplitude of leading front waves of the TSWs for the first time. The displacement of grain 399 is clearly less than that of grain 400. A separation gap between them first opens. After a while, the separation gap is closed and an overlap region between grains 399 and 400 occurs again, indicating that a second collision occurs. Then, the separation gap between

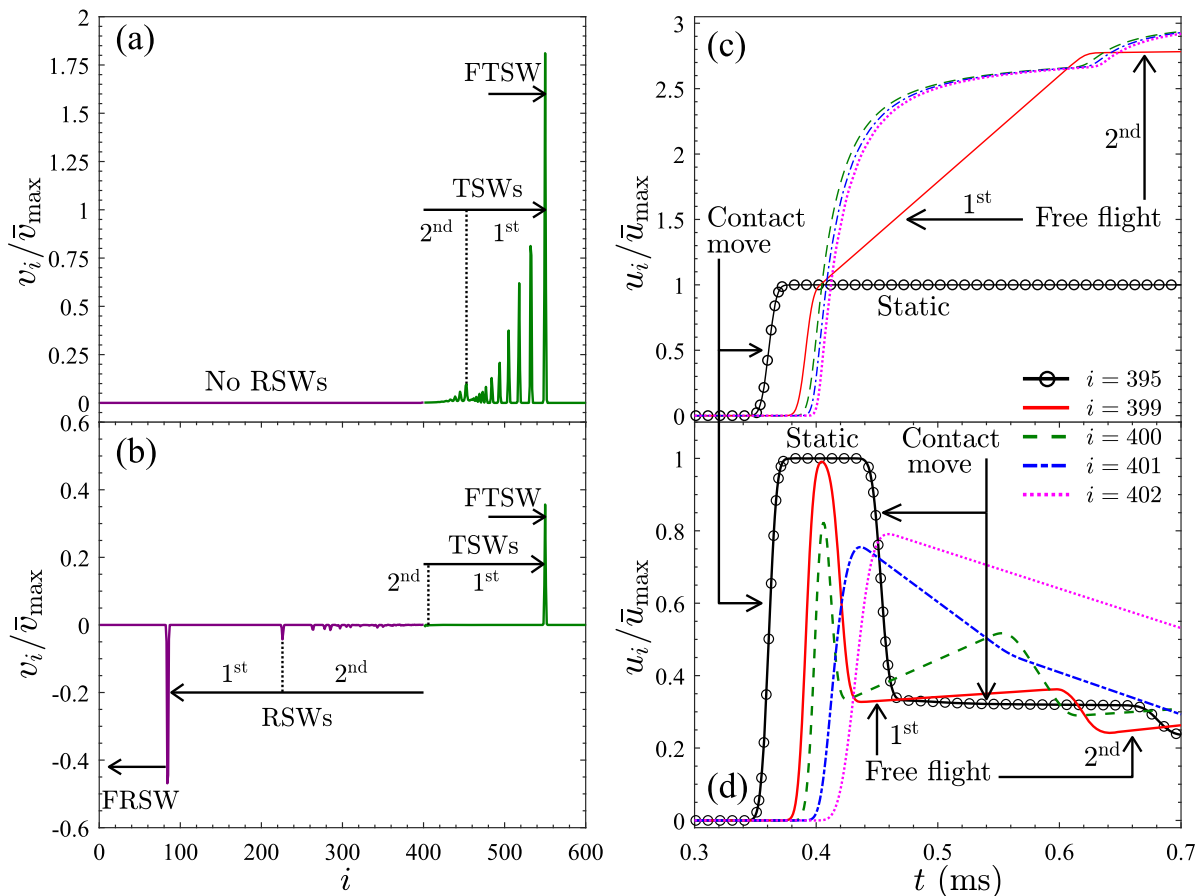


Fig. 3 (Color online) Asymmetric scattering effect in mass-mismatch granular chain with precompression $\delta_0/d = 0$. **a, b** Grain velocity as a function of grain number. **c, d** Temporal evolution of grain displacement. The results of heavy–light GC with

$\alpha_\rho = 0.2$ and light–heavy GC with $\alpha_\rho = 5$ are plotted in (a–d), respectively. The mass–mismatch interface is located at the interface of grains 400 and 401

them appears again and grain 399 enters into the 2nd free-flight mode. The two collisions between the grains of 399 and 400 are responses for the generation of two parts of TSWs, i.e., 1st and 2nd, shown in Fig. 3a. Accompanying with the opening and closing of the separation gap between grains 399 and 400, 1st- and 2nd-TSWs are produced at the same time and no RSWs are generated because of the larger grain mass of grains 399 and 400 as observed in Refs. [22, 63, 64]. Thus, the fracture only occurs in the right-section GC because the TSWs have larger wave velocity in the front part than that in the following part of ISW. The single-peak ISW breaks down and a series of multipulse-structure SWs arise in turn.

Figure 3d plots the temporal evolution of the displacement of grains around the interface for light–heavy GC with $\alpha_\rho = 5$. For grain 395, the forward contact-move and static modes occur in sequence at the beginning when the ISW passes by. A backward contact-move mode appears, corresponding to the backward propagating RSWs. Given the motion of grains 399 and 400, we can see that the forward and backward contact-move modes appear in sequence. Then, they enter into the free-flight mode. The grains of 401 and 402 show similar motions, in which the backward free-flight mode occurs just after the forward contact-move mode. The occurrence of the free-flight mode means that the separation gap appears between the adjacent grains. The nonlinear scattering effect

occurs and the ISW is decomposed. Compared with the case of heavy–light GC shown in Fig. 3c, the two sides of the light–heavy interface have many separation gaps. Furthermore, the grains such as 401 and 402 have a negative slope, indicating that they are rebounded back to the left-section GC. These observations are consistent with the appear of SW train in the multipulse structure with tiny amplitudes shown in Fig. 3b. These results are also consistent with our previous simulation results in Y-shape GC [64]. When the ISW passes through the heavy–light interface, the FTSW is an isolated SW, and the RSWs are a SW train. Moreover, all displacements of grains in the TSWs and RSWs are smaller than those in the freely propagating SW, i.e., $u_i/\bar{u}_{\max} < 1$ for light–heavy GC.

The same simulations are performed on two-section composite GC with elastic-coefficient-mismatch interface to understand the nonlinear asymmetric scattering effect due to mismatched interface. The interface is placed between grains 200 and 201. The precompression is set to $\delta_0 = 0$. The elastic coefficient ratios are set to $\alpha_{k_n} = k_n^R/k_n^L = 0.2$ and 5 for hard–soft GC and soft–hard GC, respectively. The scattering effects shown in Fig. 4a, c and b, d are similar to those in heavy–light GC and light–heavy GC in Fig. 3a, c and b, d, respectively. For the hard–soft GC, the mismatch of acoustic velocity, $\gamma_{c_0} < 1$, leads to the squeeze of the ISW at the interface. The TSWs and the RSWs are clearly seen in Fig. 4a. Moreover, the mismatch of $\gamma_{R_G} < 1$ results in the occurrence of the overshooting effect. A train of RSWs with tiny amplitudes is observed. In Fig. 4c, the overshooting effect leads to large displacements of the grains around the interface, such as $u_i/\bar{u}_{\max} > 1$, $i = 199, 200, 201, 202$. Similarly, the opening and closing of the separation gap appear several times, as shown by the straight lines in Fig. 4c. According to the occurrence time of the opening and closing of the separation gap between grains 199 and 200, the TSWs are marked by 1st and 2nd, and the RSWs are marked by 2nd, as shown in Fig. 4a. For the soft–hard GC, the fracture occurs for the TSWs because of the mismatch of acoustic velocity $\gamma_{c_0} > 1$ and a multipulse structure appears as shown in Fig. 4b. The 1st and 2nd RSWs are composed of a series of SWs, which is similar to the results of light–heavy GC shown in Fig. 3b. However, the mismatch of acoustic impedance $\gamma_{R_G} > 1$ makes the RSWs compressive. The time evolution of grain displacement shown in

Fig. 4d is similar to that in Fig. 3d. All displacements are less than 1 although the separation gaps also appear.

Following the above simulations, we explore the nonlinear asymmetric scattering effect in a highly precompressed GC with mismatched interface in mass density and elastic coefficients. The precompression of the left-section GC is fixed at $\delta_0^L/d = 10^{-3}$. Given the slow separation between the leading FTSW and the following tail of the TSWs, a long GC with 50000 grains is used and the mismatched interface is placed at the position between grains 35000 and 35001. In Fig. 5, grain velocity is plotted as a function of grain number when the FTSW arrives at grain 49900.

When the GC is a heavy–light one shown in Fig. 5a, $\alpha_\rho = 0.2$, the fracture of the ISW occurs and the TSWs are a multipulse structure as expected because of $\gamma_{c_0} > 1$. Similar to the case of $\delta_0 = 0$ in Fig. 3a, both the FTSW and the following tailed SW-like trains can propagate stably along the GC. The mismatch of acoustic impedance, i.e., $\gamma_{R_G} < 1$, results in the occurrence of the overshooting effect. Unlike the appear of separation gap shown in Fig. 3c, the overlap between the adjacent grains taken by the RSWs is less than the initial precompression. Thus, a portion of initial potential energy in the left-section GC is released and enters into the right-section GC. The overshooting effect makes the amplitude of FTSW larger than that of ISW. A train of expansive oscillatory RSWs arises, as shown in Fig. 5a. No single-peak SW is observed even if the simulation time is extended. These oscillatory RSWs cannot exist for a long time. The occupied region of the RSWs is extended, and the amplitudes decrease continuously with an increase in propagation distance.

When the interface becomes a light–heavy one, $\alpha_\rho = 5$, the squeeze effect of the ISW occurs at the interface because of $\gamma_{c_0} < 1$. Thus, the TSWs and the RSWs are compressive waves, as shown in Fig. 5b. Both of them are composed of a single leading SW and a train of continuous oscillatory wave trains. No dispersion occurs for the TSWs, which maintain their amplitude and velocity stably. However, the occupied region of the TSWs extends and the grain velocity decrease gradually. Thus, the separation distance between the frontier wave and the following tail waves increases continuously.

In Fig. 5c, the GC has a hard–soft interface with $\alpha_{k_n} = 0.2$, which corresponds to $\gamma_{c_0} < 1$ and $\gamma_{R_G} < 1$. The squeeze and the overshooting effects occur at the mismatched interface. The TSWs are compressive

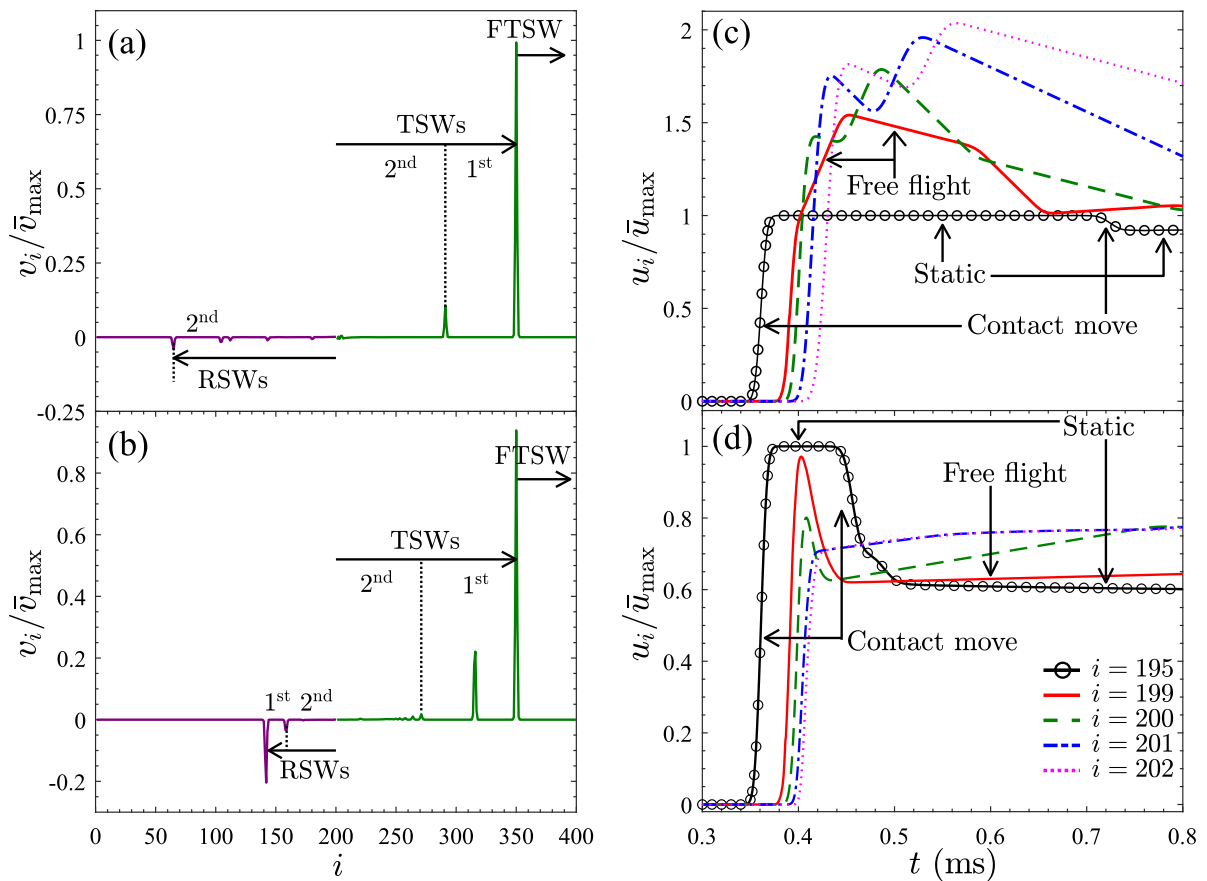


Fig. 4 (Color online) Asymmetric scattering effect in elastic-coefficient-mismatch granular chain with precompression $\delta_0/d = 0$. **a, b** Grain velocity as a function of grain number. **c, d** Temporal evolution of grain displacement. The results of

hard-soft GC with $\alpha_{k_n} = 0.2$ and soft-hard GC with $\alpha_{k_n} = 5$ are plotted in **(a, c)** and **(b, d)**, respectively. The elastic-coefficient-mismatch interface is located between grains 200 and 201

waves, which have a single leading FTSW and a train of continuous oscillatory waves. The RSWs are expansive waves, which are spreading through the GC and are dying away progressively.

In Fig. 5d, the GC is a soft-hard one with $\alpha_{k_n} = 5$, which corresponds to $\gamma_{c_0} > 1$ and $\gamma_{R_G} > 1$. As expected, the ISW is decomposed into an FTSW and a multipulse structure SWs, which can exist stably. For the RSWs, the soft characteristic of the left-section GC produces a compressive RSWs, composed of a stable FRSW and a train of oscillatory waves dying away.

The above simulation results show that the nonlinear asymmetric scattering effect can be modulated by the material parameters of two-section composite GC, i.e., mass density and elastic coefficient. The ratio of the wave velocity of FTSW to c_0^L is plotted as a function

of α_ρ and α_{k_n} in semilogarithm form to validate the dominated action of c_0 in Eq. (5), as shown in Fig. 6. The simulation results coincide well with the theoretical predictions. A monodisperse decrease (increase) in the velocity of FTSW is expected with an increase in $\log \alpha_\rho$ ($\log \alpha_{k_n}$). The good agreement observed between the simulation and theoretical results provides a solid basis for the subsequent discussions on the nonlinear scattering effect at the mismatched interface. In Fig. 7, a complete quantitative description of the nonlinear asymmetric scattering effect for the two-section composite GC is plotted in α_ρ and α_{k_n} phase space. The upward and downward triangles denote the ratios of acoustic velocity $\gamma_{c_0} = 1$ and acoustic impedance $\gamma_{R_G} = 1$, respectively. The simulation results support the theoretical predictions. The mismatch of the intrinsic

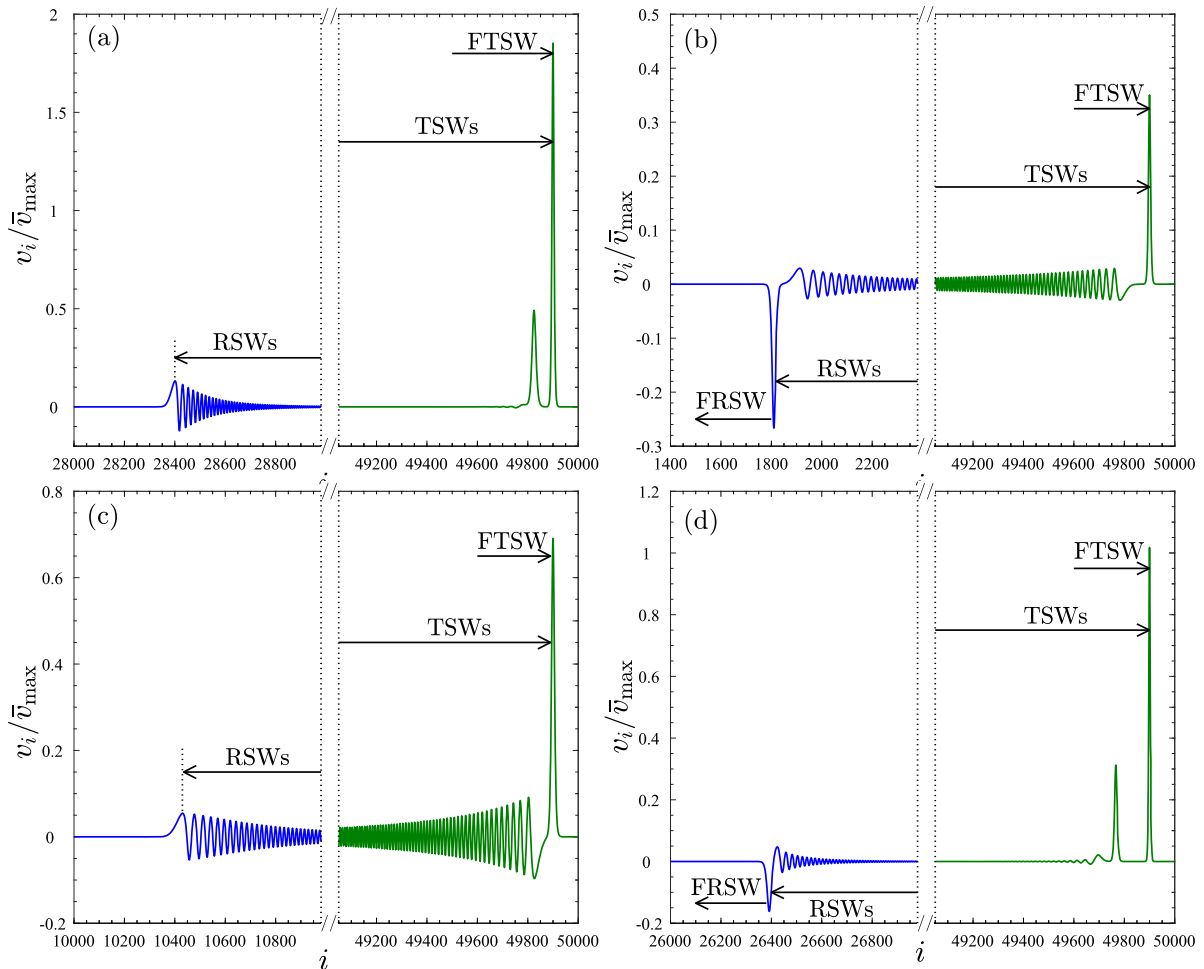


Fig. 5 (Color online) Grain velocity as a function of grain number for a precompressed GC, $\delta_0^L/d = 10^{-3}$. **a, b** are for heavy–light GC with $\alpha_\rho = 0.2$ and light–heavy GC with $\alpha_\rho = 5$,

respectively. **c, d** are for hard–soft GC with $\alpha_{k_n} = 0.2$ and soft–hard GC with $\alpha_{k_n} = 5$, respectively

sic wave dynamics leads to the occurrence of nonlinear asymmetric scattering effect. The wave characteristics of TSWs and RSWs are divided into two species, respectively. For $\gamma_{c_0} > 1$, i.e., (I) and (II) regions, the fracture effect occurs, thereby making the TSWs a multipulse structure. The FTSW is followed by a train of isolated SWs. Points (a) and (d) correspond to two typical results shown in Fig. 6a, d, respectively. In (III) and (IV) regions, i.e., $\gamma_{c_0} < 1$, the squeeze effect happens, and the TSWs are composed of a stable FTSW and a train of oscillatory waves that diminish. Two typical results are the points (b) and (c) corresponding to Fig. 6b, c, respectively. As for the RSWs, the points of

(a)(c) and (b)(d) denote the typical results of Fig. 6a, c and b, d, respectively. When $\gamma_{R_G} < 1$, i.e., (I) and (IV) regions, the interface is a hard–soft one and the overshoot effect occurs. The expansive RSWs arise, which die away gradually. However, the interface is a soft–hard one when $\gamma_{R_G} > 1$, i.e., (II) and (III) regions. The RSWs are expansive waves in the interface. A stable FTSW forms. Then, oscillatory waves die away.

The above explorations of the ratios of acoustic velocity γ_{c_0} and acoustic impedance γ_{R_G} on the nonlinear asymmetric scattering effect indicate that the phase diagram in the space of $\gamma_{c_0} - \gamma_{R_G}$ can be further divided into four subregions because of the coupling

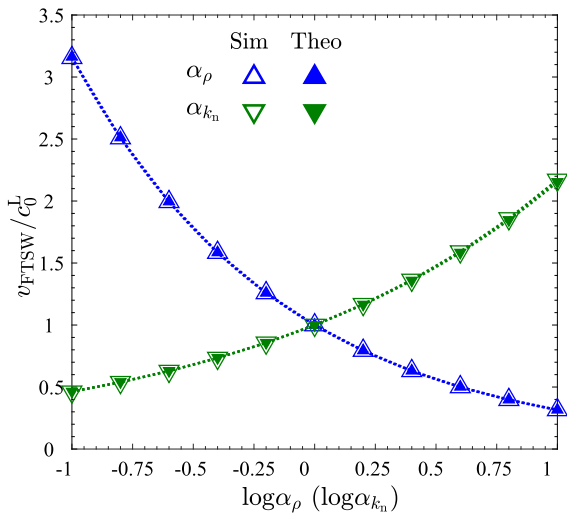


Fig. 6 (Color online) Reduced FTSW velocity by c_0^L as a function of α_ρ and α_{k_n} in semilogarithm form. The precompression is set to $\delta_0^L/d = 10^{-3}$. Upward and downward triangles are for the results of α_ρ and α_{k_n} , respectively. The open and solid symbols denote the simulation results and theoretical predictions of Eq. (5), respectively. The dashed lines are guided for eyes

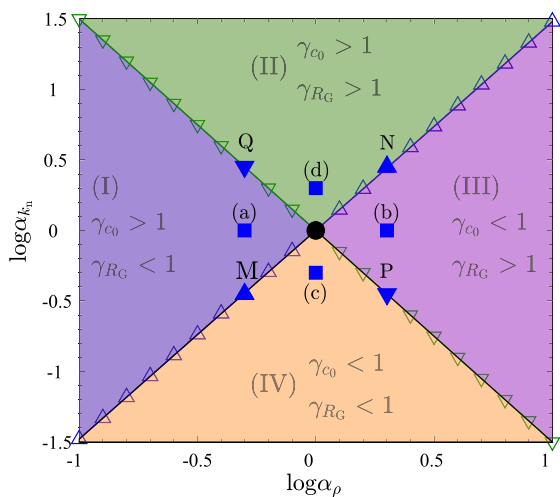


Fig. 7 (Color online) Phase diagram in α_ρ and α_{k_n} space for the nonlinear asymmetric scattering effect of SW in two-section composite GC with mismatched interface. The precompression is set to $\delta_0^L/d = 10^{-3}$. Solid circle denotes monodisperse GC. Open upward and downward triangles denote the ratios of wave velocity $\gamma_{c_0} = 1$ and acoustic impedance $\gamma_{R_G} = 1$, respectively. Solid circle denotes monodisperse GC. Points (a–d) correspond to Fig. 5a–d, respectively. Points M, N, P, Q correspond to Fig. 8a–d, respectively

effect shown in Fig. 7. Points (a)(b)(c)(d) correspond to the typical results shown in Fig. 5a–d, respectively. The fracture and the overshooting effects occur simultaneously by taking point (a) as an example, where $\gamma_{c_0} > 1$ and $\gamma_{R_G} < 1$ are located in region (I). The former makes the TSWs a multiple structure of SWs, and the latter makes the RSWs an expansive wave as shown in Fig. 5a. In Fig. 7, the GC is monodisperse when $\gamma_{c_0} = 1$ and $\gamma_{R_G} = 1$. Moreover, the ISW propagates freely along the whole chain without any scattering. Observing the scattering effect when the ratios of mass density and elastic coefficient just fall on the boundary lines is noteworthy, i.e., $\gamma_{c_0} = 1$ and $\gamma_{R_G} = 1$. The precompression is set to $\delta_0^L/d = 10^{-3}$. For the convenience of comparison, the mismatched interface is placed at the position between grains 200 and 201. The spatiotemporal evolutions of grain energy are plotted in Fig. 8, in which Fig. 8a–d corresponds to the points of M, N, P, Q in Fig. 7, respectively. The subscripts 1,2,3 denote the ratios of reduced grain kinetic energy (e_k/e_{k_0}), potential energy (e_p/e_{p_0}) and total energy (e_t/e_{t_0}), respectively. e_{k_0} , e_{p_0} , e_{t_0} are the single grain kinetic energy, potential energy, and total energy at the peak of the ISW. The corresponding data are listed in Table 2.

When $\gamma_{c_0} = 1$, the wave velocity of TSWs is expected to be equal to that of the ISW. The mismatch of acoustic impedance leads to the breakdown of the ISW. The TSWs and the RSWs are observed in Fig. 8a₁–a₃ and b₁–b₃. The quantitative energy transmission and reflection ratios are listed in Table 2 at points M and N. For a hard–soft interface, i.e., $\gamma_{R_G} = 0.5$, the overshoot effect occurs when the ISW passes through the interface. The grains around the left interface such as grains of 199 and 200 can gain considerable grain kinetic energy, as shown by a bright spot in Fig. 8a₁. The TSWs inherit the majority of the ISW’s kinetic energy, resulting in only a small amount of kinetic energy remaining in the RSWs. However, a dark spot appears for the potential energy shown in Fig. 8a₂. Then, the TSWs become brighter than the ISW. Its potential energy even exceeds that of the latter, indicating that a larger compression occurs in the right-section GC. The RSWs comprise a dark line, indicating that an expansive wave arises in the left-section GC, its potential energy is less than the initial precompressed potential energy. The spatiotemporal evolution of the ratio of total grain energy is also plotted in Fig. 8a₃. The change in the potential energy owing to the overshooting effect dom-

inates the energy scattering process, where a brighter line and a darker line arise for the TSWs and the RSWs, respectively. The energy transmission rate of the total energy $E_{\text{Tr}}^t/E_{\text{In}}^t > 1$, whereas the reflection rate $E_{\text{Re}}^t/E_{\text{In}}^t < 0$. This finding indicates that a portion of initial potential energy in the left-section GC is released and transmitted into the right-section GC. When the interface is a soft–hard one, i.e., $\gamma_{RG} = 2$, a dark spot and a bright spot appear at the left side of the interface, respectively, as shown in Fig. 8b₁, b₂. This observation implies that the interface is compressive when the ISW is passing through the interface. Thus, the TSWs and the RSWs are compressive waves shown by bright lines. Figure 8b₃ shows that the spatiotemporal evolution of total energy has more similarity with potential energy compared with that of the kinetic energy. This finding indicates that the change in potential energy also has considerable influence on the energy scattering process for the soft–hard case. This characteristic is further supported by the detailed quantitative results obtained in Table 2.

When $\gamma_{RG} = 1$, no reflection is observed and total transmission occurs as shown in the panels of Fig. 8c, d. The energy of the ISW passes through the interface completely without encountering any significant obstacles. The ratio of energy in the TSWs and RSWs to the ISW can also be found in Table 2 at points P and Q. The expected lower and higher wave velocities of the TSWs are obtained for $\gamma_{c_0} = 0.5$ and $\gamma_{c_0} = 2$, respectively. In Fig. 8c₁ – c₃, we can see that the TSWs have brighter lines than the ISW, indicating that the grains in the TSWs have large grain kinetic energy, potential energy, and total energy. The TSWs are more compact than the ISW, according to energy conversation. When $\gamma_{c_0} = 2$, the scattering effect is reversed, as shown in Fig. 8d₁ – d₃. The occupied region of the TSWs is extended compared with that of the ISW. Thus, the TSWs are darker than the ISW.

5 Conclusions

In this study, the asymmetric scattering effect of SW in a two-section composite GC is studied via numerical simulations. Building upon Nesterenko's work on solitary waves in monodisperse granular chains and using continuous acoustic wave theory in linear medium, we argue the intrinsic materials properties, i.e., mass density and elastic coefficient, dominate the asymmet-

ric scattering effect of the mismatched interface. The numerical simulations are then conducted on granular chain. The major findings are summarized as follows.

- The Nesterenko work on the characteristics of SW in monodisperse GC is briefly revisit at the unprecompressed and compressed conditions. According to continuous acoustic wave theory in a linear medium, the mismatched acoustic velocity and the impedance at the interface are used to explain the asymmetric scattering effect of the two-section GC. When the SW is incident from the section with a small acoustic velocity, the fracture effect occurs, and the TSWs are generated in a multipulse structure. On the contrary, the squeeze effect occurs at the mismatched interface with large–small acoustic velocity, in which the transmitted and reflected waves being compressive can be generated. However, the mismatched interface with high–low acoustic impedance leads to the occurrence of the overshooting effect, in which the RSWs appear as an expansive wave.
- The simulation results confirm that the mismatched acoustic velocity and the impedance at the interface, which are intrinsically determined by the mass density and elastic coefficient, dominate the nonlinear asymmetric scattering effect. When $\gamma_{c_0} > 1$, i.e., $\alpha_\rho < 1$ and $\alpha_{k_n} > 1$, the fracture effect occurs for the TSWs in which an SW train is observed. The squeeze effect occurs at the mismatched interface with $\gamma_{c_0} < 1$, i.e., $\alpha_\rho > 1$ and $\alpha_{k_n} < 1$. The overshooting effect is validated for $\gamma_{RG} < 1$. The mismatched interface, which is a hard–soft one, leads to the generation of the expansive wave in the RSWs. For the unprecompressed GC, the separation gaps arise, and the amplitude of the RSWs are very tiny. The expansive waves, which cannot live long, when the precompression is loaded. For the soft–hard interface, i.e., $\gamma_{c_0} > 1$, the RSWs propagate in the compressive form.
- The dominant effect of mass density and elastic coefficient on the characteristic wave velocities, c_0 and c_{mat} , obtains successful validation with the simulation results. An increase in the mass density and elastic coefficient can monotonically decrease and increase the velocity of the FTSW, respectively. The phase diagram in the space of $\alpha_\rho - \alpha_{k_n}$ is plotted to quantify the influence of the mismatched acoustic velocity and impedance on the nonlinear asym-

Fig. 8 (Color online) Spatiotemporal evolution of the ratios of grain kinetic energy (a_1, b_1, c_1, d_1), potential energy (a_2, b_2, c_2, d_2), and total energy (a_3, b_3, c_3, d_3) to corresponding maximum ones in the ISW. The precompression is set to $\delta_0^L/d = 10^{-3}$. The mismatched interface is placed at the position between grain 200 and 201. (a–d) correspond to the points $M(\gamma_{c_0} = 1, \gamma_{R_G} = 0.5)$, $N(\gamma_{c_0} = 1, \gamma_{R_G} = 2)$, $P(\gamma_{c_0} = 0.5, \gamma_{R_G} = 1)$, $Q(\gamma_{c_0} = 2, \gamma_{R_G} = 1)$ shown in Fig. 7, respectively

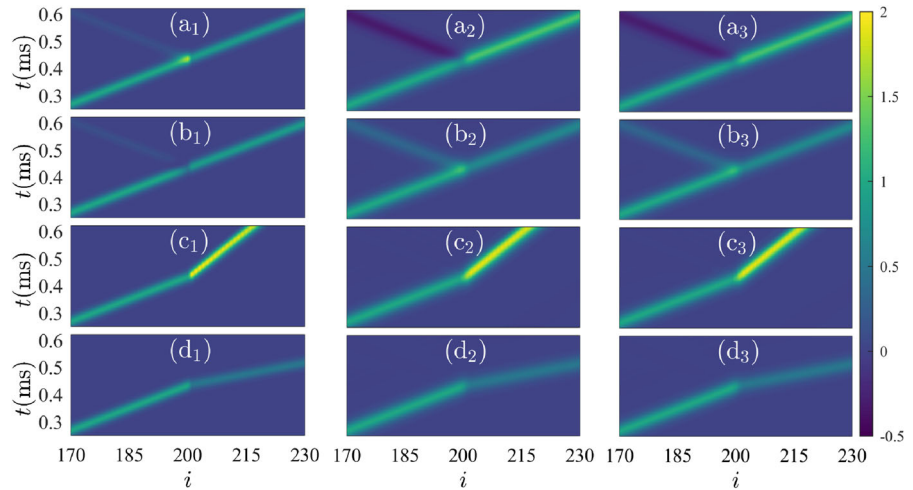


Table 2 The ratios of kinetic energy, potential energy, and total energy of the TSWs and RSWs to the ISW

Point	E_{Tr}^k/E_{In}^k	E_{Re}^k/E_{In}^k	E_{Tr}^p/E_{In}^p	E_{Re}^p/E_{In}^p	E_{Tr}^t/E_{In}^t	E_{Re}^t/E_{In}^t
M	0.88806	0.11067	1.31701	-0.31695	1.29891	-0.29891
N	0.88971	0.11089	0.67482	0.32516	0.68388	0.31612
P	0.99975	0.00023	0.99996	0.00004	0.99996	0.00004
Q	0.99997	0.00001	0.99997	0.00003	0.99997	0.00003

metric scattering effect, such as the fracture effect and the overshooting effect. Four typical contour plots clearly display the process of the nonlinear asymmetric scattering effect when $\gamma_{c_0} = 1$ and $\gamma_{R_G} = 1$, respectively. All simulation results are in good agreement with the theoretical predictions. The findings of this study pave the way to construct a novel acoustic device and a reliable nondestructive detecting method on the composite structures.

Funding This work was supported financially by the National Natural Science Foundation of China (Grant No. 11574153) and the foundation of the Ministry of Industry and Information Technology of China (Grant No. TSXK2022D007).

Data availability The datasets used and/or analyzed during the current study are available from the corresponding author on reasonable request.

Declarations

Conflict of interest The authors have no relevant financial or non-financial interests to disclose.

References

- Guo, Y., Curtis, J.S.: Discrete element method simulations for complex granular flows. *Annu. Rev. Fluid Mech.* **47**, 21 (2015)
- Hou, M., Chen, W., Zhang, T., Lu, K., Chan, C.K.: Global nature of dilute-to-dense transition of granular flows in a 2D channel. *Phys. Rev. Lett.* **91**, 204301 (2003)
- Zhou, X.Y., Liu, S.K., Zhao, Z.H., Li, X., Li, C.H., Sun, M., Huang, D.C.: Dilute-to-dense flow transition and flow-rate behavior of lateral bifurcated granular flow. *Powder Technol.* **383**, 536 (2021)
- Umbanhowar, P.B., Lueptow, R.M., Ottino, J.M.: Modeling density segregation in granular flow. *Annu. Rev. Chem. Biomol. Eng.* **10**, 5.1 (2019)
- Breu, A.P.J., Ensner, H.M., Kruelle, C.A., Rehberg, I.: Reversing the Brazil–Nut effect: competition between percolation and condensation. *Phys. Rev. Lett. Eng.* **90**, 014302 (2003)
- Shao, Y.F., Li, A.H., Wang, Z.Z., Sun, M., Huang, D.C.: Resonance–induced acceleration of the RBNE–BNE segregation inversion. *AIChE J.* e18101 (2022)
- Fronk, M.D., Fang, L., Packo, P., Leamy, M.J.: Elastic wave propagation in weakly nonlinear media and metamaterials: a review of recent developments. *Nonlinear Dyn.* **111**, 10709 (2023)
- Lydon, J., Jayaprakash, K.R., Ngo, D., Starosvetsky, Y.L., Vakakis, A.F., Daraio, C.: Frequency bands of strongly

- nonlinear homogeneous granular systems. *Phys. Rev.* **88**, 012206 (2013)
9. Jiao, T.F., Zhang, S.T., Sun, M., Huang, D.C.: Occurrence of gradual resonance in a finite-length granular chain driven by harmonic vibration. *Nonlinear Dyn.* **111**, 9049 (2023)
 10. Zhou, J.Z., McFarland, D.M., Cheng, X.L., Lu, H.C., Vakis, A.F.: One-dimensional granular chains as transmitted force attenuators. *Nonlinear Dyn.* **111**, 14713 (2023)
 11. Burgoyne, H.A., Newman, J.A., Jackson, W.C., Daraio, C.: Guided impact mitigation in 2D and 3D granular crystals. *Procedia Eng.* **103**, 52 (2015)
 12. Breindel, A., Sun, D., Sen, S.: Impulse absorption using small, hard panels of embedded cylinders with granular alignments. *Appl. Phys. Lett.* **99**, 063510 (2011)
 13. Boechler, N., Theocharis, G., Daraio, C.: Bifurcation-based acoustic switching and rectification. *Nat. Mater.* **10**, 665 (2011)
 14. Li, F., Anzel, P., Yang, J., Kevrekidis, P.G., Daraio, C.: Granular acoustic switches and logic elements. *Nat. Commun.* **5**, 5311 (2014)
 15. Liu, Y.F., Qin, Z.Y., Chu, F.L.: Nonlinear forced vibrations of FGM sandwich cylindrical shells with porosities on an elastic substrate. *Nonlinear Dyn.* **104**, 1007 (2021)
 16. Liu, Y.F., Qin, Z.Y., Chu, F.L.: Nonlinear forced vibrations of rotating cylindrical shells under multi-harmonic excitations in thermal environment. *Nonlinear Dyn.* **108**, 2977 (2022)
 17. Nesterenko, V.F.: Propagation of nonlinear compression pulses in granular media. *J. Appl. Mech. Tech. Phys.* **24**, 733 (1983)
 18. Nesterenko, V.F.: *Dynamics of Heterogeneous Materials*. Springer-Verlag, New York (2001)
 19. Nesterenko, V.F.: Waves in strongly nonlinear discrete systems. *Phil. Trans. R. Soc. A* **376**, 20170130 (2018)
 20. Sen, S., Hong, J.B., Bang, J.H., Avalos, E., Doney, R.: Solitary waves in the granular chain. *Phys. Rep.* **462**, 21 (2008)
 21. Rosas, A., Lindenberg, K.: Pulse propagation in granular chains. *Phys. Rep.* **735**, 1 (2018)
 22. Ngo, D., Fraternali, F., Daraio, C.: Highly nonlinear solitary wave propagation in Y-shaped granular crystals with variable branch angles. *Phys. Rev. E* **85**, 036602 (2012)
 23. Leonard, A., Ponson, L., Daraio, C.: Wave mitigation in ordered networks of granular chains. *J. Mech. Phys. Solids* **73**, 103 (2014)
 24. Liu, S.S., Yang, Y.Y., Duan, W.S., Yang, L.: Pulse reflection and transmission due to impurities in a granular chain. *Phys. Rev. E* **92**, 013202 (2015)
 25. Tzirtzilakis, E., Xenos, M., Marinakis, V., Bountis, T.C.: Interactions and stability of solitary waves in shallow water. *Chaos Solitons Fractals* **14**, 87 (2002)
 26. Chen, Y.Y., Kharif, C., Yang, J.H., Hsu, H.C., Touboul, J., Chambarel, J.: An experimental study of steep solitary wave reflection at a vertical wall. *Eur. J. Mech. B-Fluid.* **49**, 20–28 (2015)
 27. Su, C.H., Mirie, R.M.: On head-on collisions between two solitary waves. *J. Fluid Mech.* **98**, 509–525 (1980)
 28. Coste, C., Falcon, E., Fauve, S.: Solitary waves in a chain of beads under Hertz contact. *Phys. Rev. E* **56**, 6104 (1997)
 29. Manciu, M., Sen, S., Hurd, A.J.: Impulse propagation in dissipative and disordered chains with power-law repulsive potentials. *Phys. D* **157**, 226 (2001)
 30. Takato, Y., Sen, S.: Long-lived solitary wave in a precompressed granular chain. *EPL* **100**, 24003 (2015)
 31. Jiao, T.F., Chen, W.Z., Takato, Y., Sen, S., Huang, D.C.: Revisiting Nesterenko's solitary wave in the precompressed granular alignment held between fixed ends. *Granul. Matter.* **25**, 17 (2023)
 32. Chen, Y., Yeh, H.: Laboratory experiments on counter-propagating collisions of solitary waves. Part I. Wave interactions. *J. Fluid Mech.* **749**, 577 (2014)
 33. Liu, X.Y., Wen, W., Mao, X.Z., Wang, X.L.: Optimal and efficient generation of sine-Gordon breathers. *Phys. Rev. E* **104**, 014209 (2021)
 34. Jin, T., Zhao, H., Hu, B.: Spatial shift of lattice soliton scattering in the Fermi-Pasta-Ulam model. *Phys. Rev. E* **81**, 037601 (2010)
 35. Manciu, M., Sen, S.: Crossing of identical solitary waves in a chain of elastic beads. *Phys. Rev. E* **63**, 016614 (2000)
 36. Manciu, F.S., Sen, S.: Secondary solitary wave formation in systems with generalized Hertz interactions. *Phys. Rev. E* **66**, 016616 (2002)
 37. Avalos, E., Sen, S.: How solitary waves collide in discrete granular alignments. *Phys. Rev. E* **79**, 046607 (2009)
 38. Deng, G., Biondini, G., Sen, S.: Interactions of solitary waves in integrable and nonintegrable lattices. *Chaos* **30**, 043101 (2020)
 39. Tichler, A.M., Gómez, L.R., Upadhyaya, N., Campman, X., Nesterenko, V.F., Vitelli, V.: Transmission and reflection of strongly nonlinear solitary waves at granular interfaces. *Phys. Rev. Lett.* **111**, 048001 (2013)
 40. Santibanez, F., Munoz, R., Caussarieu, A., Job, S., Melo, F.: Experimental evidence of solitary wave interaction in Hertzian chains. *Phys. Rev. E* **84**, 026604 (2011)
 41. Shen, Y., Kevrekidis, P.G., Sen, S., Hoffman, A.: Characterizing traveling-wave collisions in granular chains starting from integrable limits: the case of the Korteweg-de Vries equation and the Toda lattice. *Phys. Rev. E* **90**, 022905 (2014)
 42. Ma, L., Huang, D.C., Chen, W.Z., Jiao, T.F., Sun, M., Hu, F.L., Su, Y.J.: Oscillating collision of the granular chain on static wall. *Phys. Lett. A* **381**, 542 (2017)
 43. Wu, Q.Q., Liu, X.Y., Jiao, T.F., Sen, S., Huang, D.C.: Head-on collision of solitary waves described by the Toda lattice model in granular chain. *Chin. Phys. Lett.* **37**, 074501 (2020)
 44. Zhang, S.T., Liu, S.K., Jiao, T.F., Sun, M., Hu, F.L., Huang, D.C.: Nonlinear interaction of head-on solitary waves in integrable and nonintegrable systems. [arXiv:2310.19356](https://arxiv.org/abs/2310.19356) (2023)
 45. Wen, Z.Y., Wang, S.J., Zhang, X.M., Li, L.: Solitary Wave Interactions in Granular Media. *Chin. Phys. Lett.* **24**, 2887 (2007)
 46. Avalos, E., Sun, D.K., Doney, D.L., Sen, S.: Sustained strong fluctuations in a nonlinear chain at acoustic vacuum: Beyond equilibrium. *Phys. Rev. E* **84**, 046610 (2011)
 47. Vergara, L.: Scattering of solitary waves from interfaces in granular media. *Phys. Rev. Lett.* **95**, 108002 (2005)
 48. Nesterenko, V.F., Daraio, C., Herbold, E.B., Jin, S.: Anomalous wave reflection at the interface of two strongly nonlinear granular media. *Phys. Rev. Lett.* **95**, 158702 (2005)
 49. Daraio, C., Ngo, D., Nesterenko, V.F., Fraternali, F.: Highly nonlinear pulse splitting and recombination in a two-

- dimensional granular network. *Phys. Rev. E* **82**, 036603 (2010)
50. Herbold, E.B., Nesterenko, V.F.: Propagation of rarefaction pulses in discrete materials with strain-softening behavior. *Phys. Rev. Lett.* **110**, 144101 (2013)
 51. Wang, P.J., Xia, J.H., Li, Y.D., Liu, C.S.: Crossover in the power-law behavior of confined energy in a composite granular chain. *Phys. Rev. E* **76**, 041305 (2007)
 52. Wallen, S.P., Lee, J., Mei, D., Chong, C., Kevrekidis, P.G., Boechler, N.: Discrete breathers in a mass-in-mass chain with Hertzian local resonators. *Phys. Rev. E* **95**, 022904 (2017)
 53. Yang, Y.Y., Liu, S.W., Zhang, Z.B., Duan, W.S., Yang, L.: Solitary waves propagation described by Korteweg-de Vries equation in the granular chain with initial prestress. *AIP Adv.* **6**, 075317 (2016)
 54. Przedborski, M., Harroun, T.A., Sen, S.: Granular chains with soft boundaries: slowing the transition to quasiequilibrium. *Phys. Rev. E* **91**, 042207 (2015)
 55. Kinsler, L.E., Frey, A.R., Coppens, A.B., Sanders, J.V.: *Fundamentals of Acoustics*. John Wiley (1999)
 56. Du, G.H., Zhu, Z.M., Gong, F.X.: *Fundamentals of Acoustics*. Nanjing University Press (2012)
 57. Cundall, P.A., Strack, O.D.L.: A discrete numerical model for granular assemblies. *Geotechnique* **29**, 47 (1979)
 58. Kuwabara, G., Kono, K.: Restitution coefficient in a collision between two spheres. *Japn. J. Appl. Phys.* **26**, 1230 (1987)
 59. Schäfer, J., Dippel, S., Wolf, D.E.: Force schemes in simulations of granular materials. *J. Phys. I*, **6**, 5 (1996)
 60. Xu, Y., Nesterenko, V.F.: Propagation of short stress pulses in discrete strongly nonlinear tunable metamaterials. *Philos. Trans. R. Soc. A* **372**, 20130186 (2014)
 61. Daraio, C., Herbold, E.B., Nesterenko, V.F., Jin, S.: Energy trapping and shock disintegration in a composite granular medium. *Phys. Rev. Lett.* **96**, 058002 (2006)
 62. Sen, S., Manciu, M., Wright, J.D.: Solitonlike pulses in perturbed and driven Hertzian chains and their possible applications in detecting buried impurities. *Phys. Rev. E* **57**, 2386 (1998)
 63. Sokolow, A., Bittle, E.G., Sen, S.: Solitary wave train formation in Hertzian chains. *EPL* **77**, 24002 (2007)
 64. Liu, X.Y., Jiao, T.F., Ma, L., Su, J.Y., Chen, W.Z., Sun, Q.C., Huang, D.C.: Rectification effect on solitary waves in the symmetric Y-shaped granular chain. *Granul. Matt.* **19**, 55 (2017)

Publisher's Note Springer Nature remains neutral with regard to jurisdictional claims in published maps and institutional affiliations.

Springer Nature or its licensor (e.g. a society or other partner) holds exclusive rights to this article under a publishing agreement with the author(s) or other rightsholder(s); author self-archiving of the accepted manuscript version of this article is solely governed by the terms of such publishing agreement and applicable law.